Acta Crystallographica Section D
Biological Crystallography
ISSN 0907-4449

Complexes of *Thermotoga maritima* *S*-adenosylmethionine decarboxylase provide insights into substrate specificity

Shridhar Bale,[a] Kavita Baba,[a] Diane E. McCloskey,[b] Anthony E. Pegg[b] and Steven E. Ealick[a]*

[a]Department of Chemistry and Chemical Biology, Cornell University, Ithaca, New York 14853, USA, and [b]Departments of Cellular and Molecular Physiology and of Pharmacology, Milton S. Hershey Medical Center, Pennsylvania State University College of Medicine, Hershey, Pennsylvania 17033, USA

Correspondence e-mail: see3@cornell.edu

Received 30 September 2009
Accepted 16 November 2009

PDB References: *S*-adenosylmethionine decarboxylase, 3iwb; complex with *S*-adenosylmethionine methyl ester, 3iwc; complex with 5′-deoxy-5′-dimethylthioadenosine, 3iwd.

The polyamines putrescine, spermidine and spermine are ubiquitous aliphatic cations and are essential for cellular growth and differentiation. *S*-Adenosylmethionine decarboxylase (AdoMetDC) is a critical pyruvoyl-dependent enzyme in the polyamine-biosynthetic pathway. The crystal structures of AdoMetDC from humans and plants and of the AdoMetDC proenzyme from *Thermotoga maritima* have been obtained previously. Here, the crystal structures of activated *T. maritima* AdoMetDC (TmAdoMetDC) and of its complexes with *S*-adenosylmethionine methyl ester and 5′-deoxy-5′-dimethylthioadenosine are reported. The results demonstrate for the first time that TmAdoMetDC autoprocesses without the need for additional factors and that the enzyme contains two complete active sites, both of which use residues from both chains of the homodimer. The complexes provide insights into the substrate specificity and ligand binding of AdoMetDC in prokaryotes. The conservation of the ligand-binding mode and the active-site residues between human and *T. maritima* AdoMetDC provides insight into the evolution of AdoMetDC.

1. Introduction

S-Adenosylmethionine decarboxylase (AdoMetDC) is a critical enzyme at a key branch point in the polyamine-biosynthetic pathway (Hackert & Pegg, 1997; Pegg *et al.*, 1998; Tabor & Tabor, 1984*a*,*b*). AdoMetDC catalyzes the decarboxylation of *S*-adenosylmethionine (AdoMet) to *S*-adenosyl-5′-(3-methylthiopropylamine) (dcAdoMet). The propylamine group of dcAdoMet is transferred to either putrescine or spermidine to form spermidine or spermine, respectively. The primary role of AdoMet in cells is as a methyl-group donor to a variety of substrates or as a cofactor or cosubstrate for radical AdoMet enzymes (Frey *et al.*, 2008). However, after decarboxylation dcAdoMet is committed to polyamine biosynthesis. The polyamines putrescine, spermidine and spermine are ubiquitous across all forms of life and are implicated in cellular growth and differentiation. Elevated levels of polyamines are associated with various tumors and parasitic diseases (Gerner & Meyskens, 2004; Pegg, 1988). Consequently, AdoMetDC and other enzymes in the polyamine-biosynthetic pathway are promising targets for proliferative diseases (Casero *et al.*, 2005; Casero & Marton, 2007).

AdoMetDC is expressed as a proenzyme and undergoes an internal serinolysis reaction as part of a post-translational modification to generate the active-site pyruvoyl group. This process cleaves the peptide chain to α and β chains, with the

pyruvoyl group being generated at the N-terminus of the α chain. The α chain is derived from the carboxy end of the proenzyme and the β chain is derived from the amino end of the proenzyme. The crystal structures of wild-type human AdoMetDC (hAdoMetDC) and of H243A and S68A mutants provided insights into the mechanism of autoprocessing of the enzyme (Ekstrom *et al.*, 1999, 2001; Tolbert *et al.*, 2003). The crystal structures of AdoMetDC from plants and of the AdoMetDC proenzyme from *Thermotoga maritima* have also been determined (Bennett *et al.*, 2002; Toms *et al.*, 2004). The dimeric fold of *T. maritima* AdoMetDC (TmAdoMetDC) is similar to the monomeric protomers of human and plant AdoMetDC, suggesting evolutionary links involving gene duplication and fusion.

The crystal structure of the human enzyme has been determined complexed with various ligands and substrate analogues (McCloskey *et al.*, 2009; Tolbert *et al.*, 2001). The complex of hAdoMetDC with *S*-adenosylmethionine methyl ester (MeAdoMet) revealed key interactions of the ligand with the active-site residues and the binding conformation of the ligand. MeAdoMet forms a Schiff base with the pyruvoyl group and the adenine base binds in an unusual *syn* conformation that is stabilized by stacking interactions with Phe223 and Phe7 and hydrogen bonds to Glu67. The hydroxyl groups of the ribose make two hydrogen bonds to Glu247. The crystal structures of the inactive proenzyme of TmAdoMetDC and of the S63A mutant, which lacks the serine required for autoprocessing, have been reported previously (Toms *et al.*, 2004). In this paper, we report the crystal structure of processed fully active TmAdoMetDC and of its complexes with MeAdoMet and 5′-deoxy-5′-dimethylthioadenosine (MMTA). We compare the complexes of TmAdoMetDC with the complexes of hAdoMetDC. The comparison and the conservation of the active-site residues reveal recurring themes for substrate recognition and catalysis.

2. Materials and methods

2.1. Protein expression, processing and purification

The expression and purification protocol of TmAdoMetDC has been described previously (Toms *et al.*, 2004). Briefly, *Escherichia coli* B834(DE3) cells were transformed with the pTmSpeD.28 plasmid. A 10 ml overnight starter culture was grown in LB medium supplemented with 35 μg ml^{-1} kanamycin. It was then introduced into 1 l cell culture, grown until the OD_{600} reached 0.6 and subsequently induced with 1 m*M* isopropyl β-D-1-thiogalactopyranoside. The temperature was reduced to 288 K and the protein was expressed overnight. The cells were harvested by centrifugation and were stored at 193 K.

The cells were suspended in a wash buffer consisting of 50 m*M* Tris–HCl pH 8.0, 10 m*M* imidazole and 500 m*M* NaCl and lysed using a sonicator. To induce conversion of the proenzyme to the fully active processed enzyme, the lysate was heated at 353 K for 1 h. The heating process also served as a partial purification step. The lysate was centrifuged and the supernatant was passed through an Ni–NTA column equilibrated with wash buffer. The column was washed with 100 ml wash buffer followed by 50 ml of buffer containing 50 m*M* Tris–HCl pH 8.0, 35 m*M* imidazole and 500 m*M* NaCl. The protein was eluted with elution buffer containing 50 m*M* Tris–HCl pH 8.0, 150 m*M* imidazole and 500 m*M* NaCl and dialyzed into 20 m*M* Tris–HCl pH 8.0 and 1 m*M* dithiothreitol. The protein was concentrated to 6 mg ml^{-1} and stored at 193 K.

2.2. Crystallization conditions

The protein was crystallized using the hanging-drop vapor-diffusion method at room temperature. The crystallization conditions consisted of 2.4–2.8 *M* ammonium formate and 100 m*M* HEPES pH 8.0. Crystals appeared in two weeks and grew to maximum dimensions of 0.2 × 0.15 × 0.1 mm in 3–4 weeks. To obtain crystals of the complexes, the crystals were transferred into well solution containing either 5 m*M* MeAdoMet or MMTA for 4 h. The crystals belonged to space group *R*3 and showed minor twinning, which varied from crystal to crystal.

2.3. Data collection and processing

Data for the processed enzyme were collected at our home source on a Rigaku R-AXIS IV^{++} detector using Cu $K\alpha$ radiation from a Rigaku RU-300 rotating-anode generator. Data were collected over a range of 100° with a 0.5° oscillation angle, 15 min exposure per frame and a crystal-to-detector distance of 180 mm. Crystals of the complexes were sequentially transferred into well solution containing 5, 10, 15 and 20% glycerol and 200 m*M* ammonium formate prior to freezing in liquid nitrogen. Data for the complexes were collected on the 24-ID-E beamline at the NE-CAT sector of the Advanced Photon Source. Data were collected over 140° and 150° for the MeAdoMet and MMTA complexes, respectively, with a 1° oscillation angle, 1 s exposure per frame and a crystal-to-detector distance of 260 mm. The data were indexed, integrated and scaled using the *HKL*-2000 program suite (Otwinowski & Minor, 1997). The data-collection statistics are summarized in Table 1.

2.4. Structure determination and refinement

The structures of the processed enzyme and the complexes were solved by molecular replacement using the *CNS* program suite (Brünger *et al.*, 1998). The structure of the wild-type proenzyme (PDB code 1tlu; Toms *et al.*, 2004) was used as the search model for molecular replacement. Model building of the protein was carried out using the program *Coot* (Emsley & Cowtan, 2004). The refinement process included successive rounds of simulated annealing, *B*-factor refinement, minimization and the calculation of composite OMIT maps and difference Fourier maps. After several rounds of refinement and model building, the difference Fourier and composite OMIT maps were used to identify bound ligands (Fig. 1) and water molecules. The topology and parameter files for MeAdoMet and MMTA were obtained from the HIC-UP

server (Kleywegt & Jones, 1998). The ligand and water molecules were added to the structure and followed by a few rounds of refinement as mentioned above. The final refinement statistics are shown in Table 2.

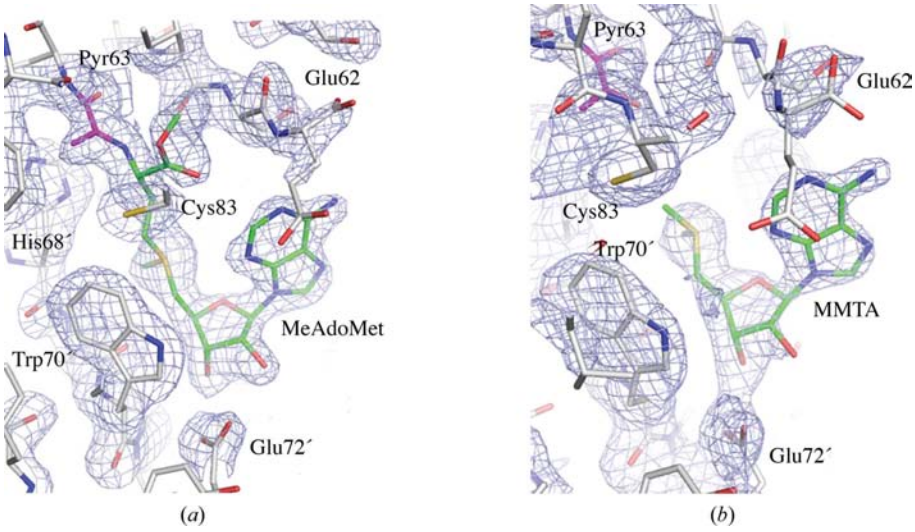

Figure 1
Electron density for TmAdoMetDC complexes. (*a*) The MeAdoMet complex. (*b*) The MMTA complex. The $F_o - F_c$ electron-density maps were calculated by omitting all residues within 4.0 Å of the ligand. The C atoms of the ligands are colored green and the C atoms of the pyruvoyl group are colored magenta. The electron density is contoured at 3σ.

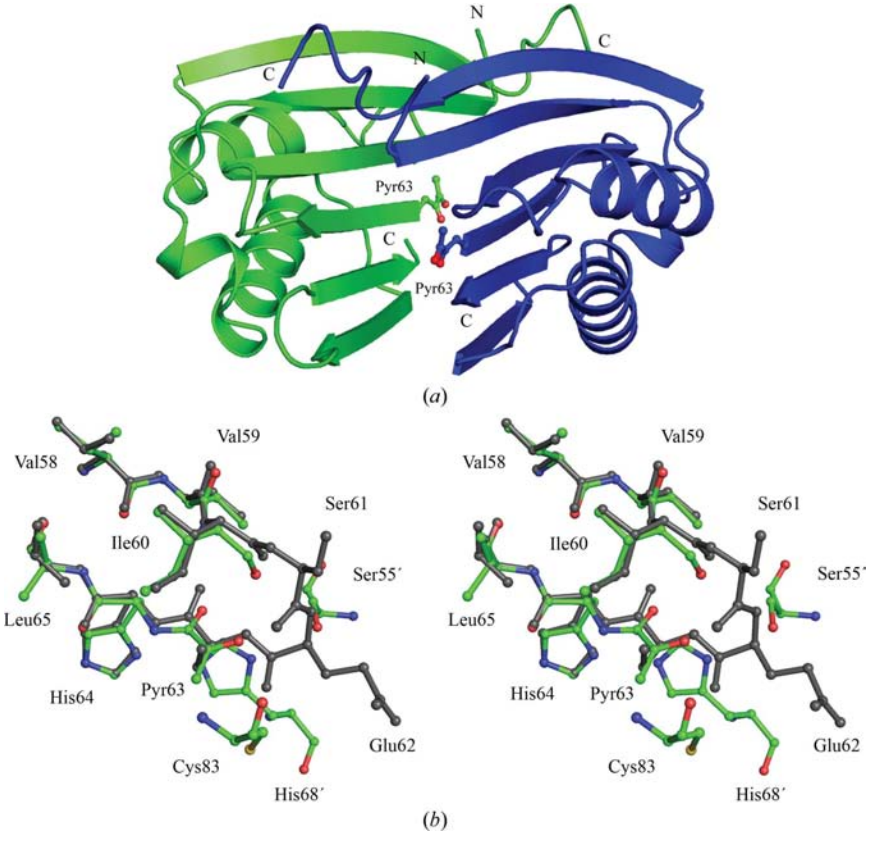

Figure 2
(*a*) Overall structure of processed TmAdoMetDC. The dimeric structure of the enzyme is shown with the monomers colored green and blue. The pyruvoyl group formed is shown in ball-and-stick representation and labeled. (*b*) Stereoview of superposition of the processed enzyme (C atoms colored green) and the proenzyme (shown in black). Residues Ser61 and Glu62 are disordered in the processed enzyme.

2.5. TmAdoMetDC kinetic measurements

TmAdoMetDC was assayed by measuring the release of $^{14}CO_2$ from *S*-adenosyl-L-[carboxy-^{14}C]methionine as described previously (Shantz & Pegg, 1998). The linear ranges for protein amount, time and temperature were determined for TmAdoMetDC and the final assay conditions for the determination of TmAdoMetDC activity, which were chosen to be within the linear range for each parameter, were as follows: 5 ng purified TmAdoMetDC, which had been heated at 353 K for 6 h to ensure complete processing, was assayed at pH 6.8 for 10 min at 338 K. For determination of the K_m for AdoMet, triplicate samples were assayed for six concentrations of AdoMet ranging from 8 to 270 μM.

2.6. Figure preparation and PDB deposition

The figures were prepared using *PyMOL* (DeLano, 2002) and *ChemDraw*. The PDB code for the processed form of TmAdoMetDC is 3iwb, that for the complex with MeAdoMet is 3iwc and that for the complex with MMTA is 3iwd.

3. Results

3.1. Overall structure of processed enzyme

The TmAdoMetDC proenzyme does not appear to process at room temperature; however, heating the crude lysate to 353 K for 1 h yielded fully processed enzyme. The overall structure of the processed enzyme in the asymmetric unit is a homodimer with twofold noncrystallographic symmetry (Fig. 2*a*). The protomer, which consists of one α chain and one β chain, forms a two-layer $\alpha\beta$ sandwich with an antiparallel β-sheet flanked on one side by two α-helices. The protomer fold is similar to that of the proenzyme. The dimer interface is formed by the interaction of the β-sheets of the protomers. The autoprocessing reaction occurs

Table 1
Summary of data-collection and processing statistics.

Values in parentheses are for the highest resolution shell.

	TmAdoMetDC, processed	TmAdoMetDC + MeAdoMet	TmAdoMetDC + MMTA
Wavelength (Å)	1.5418	0.9792	0.9792
Space group	*R*3	*R*3	*R*3
Unit-cell parameters (Å)			
a	104.71	105.20	105.47
c	69.84	70.06	70.11
Resolution (Å)	2.06	1.90	1.90
Total reflections	49357	91891	101615
Unique reflections	16833	22459	22388
Redundancy	2.9 (1.7)	4.1 (2.3)	4.5 (2.8)
Completeness (%)	95.4 (71.2)	98.9 (90.4)	97.6 (79.6)
$I/\sigma(I)$	23.1 (4.1)	17.9 (3.1)	24.4 (2.9)
$R_{\rm merge}$†	4.5 (21.0)	9.6 (21.6)	6.5 (23.6)
Matthews coefficient (Å^3 Da^{-1})	2.49	2.52	2.54
Solvent content (%)	49.7	50.3	50.8

† $R_{\rm merge} = \sum_{hkl}\sum_i |I_i(hkl) - \langle I(hkl)\rangle| / \sum_{hkl}\sum_i I_i(hkl)$, where $\langle I(hkl)\rangle$ is the mean intensity of the i reflections with intensities $I_i(hkl)$ and common indices hkl.

Table 2
Refinement statistics for processed TmAdoMetDC and complexes.

	TmAdoMetDC, processed	TmAdoMetDC + MeAdoMet	TmAdoMetDC + MMTA
Resolution (Å)	2.06	1.90	1.90
R factor†	0.233	0.212	0.249
$R_{\rm free}$‡	0.262	0.238	0.280
No. of non-H atoms			
Protein	1868	1917	1900
Ligand	—	56	42
Water	115	108	61
B factors (Å^2)			
Protein	28.3	33.5	31.0
Ligand	—	54.6/44.4	46.1/41.9
R.m.s. deviations			
Bonds (Å)	0.011	0.031	0.006
Angles (°)	1.4	1.5	1.2
Dihedrals (°)	25.0	27.2	25.3
Ramachandran plot (%)			
Most favored region	94.5	95.6	95.6
Additional allowed region	5.5	4.4	4.4
Disallowed region	0.0	0.0	0.0

† *R* factor = $\sum_{hkl} ||F_{\rm obs}| - |F_{\rm calc}|| / \sum_{hkl} |F_{\rm obs}|$, where $F_{\rm obs}$ and $F_{\rm calc}$ are the observed and calculated structure factors, respectively. ‡ For $R_{\rm free}$, the sum extends over a subset of reflections (5% for processed TmAdoMetDC and 10% for the TmAdoMetDC–MeAdoMet and TmAdoMetDC–MMTA complexes) that were excluded from all stages of refinement.

between residues Glu62–Ser63, which are located in a β-turn consisting of residues Ile60–Ser63. The electron-density maps show a clear break in the main-chain density and the formation of a pyruvoyl group at position 63. Residues Ser61 and Glu62 are disordered in the processed enzyme but become ordered upon ligand binding (see below). The active site is at the dimer interface and contains residues from both protomers. A comparison of the processed structure and the proenzyme shows no significant change in the overall secondary structure. A stereoview of the comparison of the proenzyme and the processed enzyme at the processing site is shown in Fig. 2(*b*).

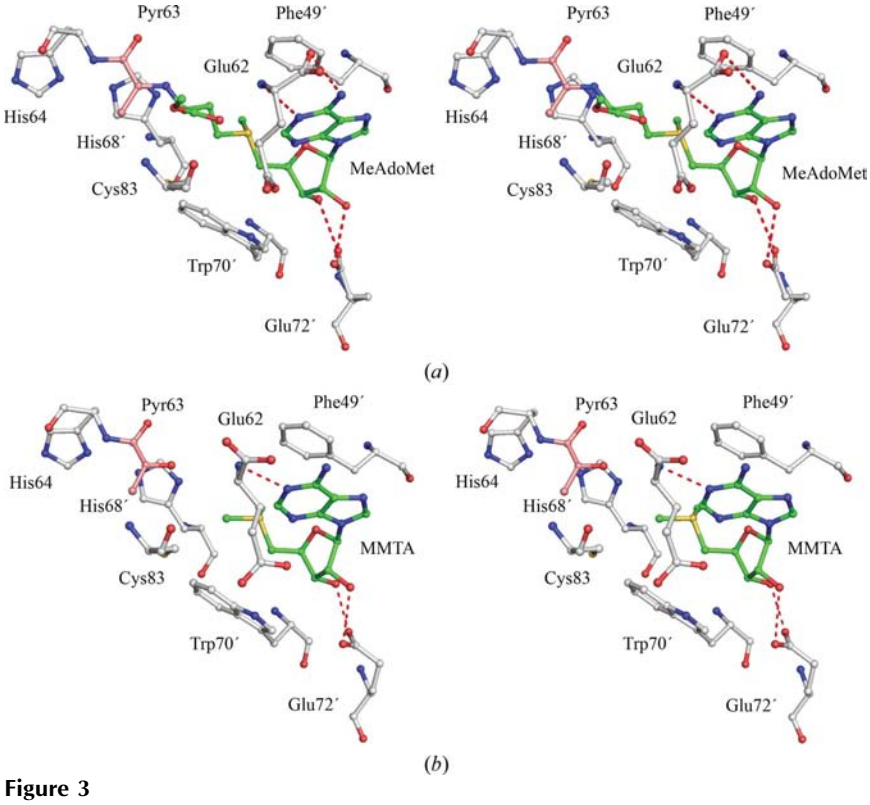

Figure 3
Complexes of TmAdoMetDC. (*a*) Stereoview of MeAdoMet covalently bound to the enzyme. The pyruvoyl group has C atoms colored pink and MeAdoMet has C atoms colored green. (*b*) Stereoview of MMTA bound to the enzyme. The pyruvoyl group has C atoms colored pink and MMTA has C atoms colored green. Hydrogen bonds are shown as dashed lines.

3.2. Complex with MeAdoMet

The crystal structure of TmAdoMetDC complexed with MeAdoMet was solved by molecular replacement. The difference $F_{\rm o} - F_{\rm c}$ density shows that MeAdoMet binds to each protomer and forms a Schiff base with the active-site pyruvoyl group (Fig. 1*a*). Each active site utilizes residues from both protomers. The 2′ and 3′ O atoms of the ribose form hydrogen bonds to the carboxylate group of Glu72′ (residues marked with a prime are from the twofold-related protomer). The adenine base of MeAdoMet binds in the unusual *syn* conformation, stacking against Phe49′. The χ_1 torsion angle of Phe49′ undergoes a rotation of 90° compared with the unliganded enzyme, allowing its side chain to stack against the adenine base. In addition, the χ_1 torsion angle of His47′ rotates by 130°, allowing edge-to-face stacking with Phe49′. Residues Ser61 and Glu62 become ordered upon binding of MeAdoMet. The N6 and N1 atoms of the adenine base make

two hydrogen bonds to the Glu62 carboxylate and amide groups, respectively. The sulfonium ion of MeAdoMet is sandwiched between the aromatic rings of Phe49′ and Trp70′. The sulfonium ion is 4.4 Å from the CZ2 atom of the tryptophan ring, which is also the closest contact of the sulfonium with Trp70′. The sulfonium ion is 4.7 Å away from the center of the six-membered ring of tryptophan. The sulfonium ion is 4.2 Å from the center of the Phe49′ ring and 3.8 Å from the CD2 and CE2 atoms of the ring, which is also the closest contact of the sulfonium with Phe49′. These contacts suggest cation–π interactions similar to those observed in the human enzyme (Bale *et al.*, 2009). The χ_1 torsion angle Tyr52′ undergoes a rotation of 100° upon ligand binding, moving it further into the active site. Tyr52′ partially shields MeAdoMet from the external solvent. A stereoview of MeAdoMet bound to TmAdoMetDC is shown in Fig. 3(*a*). A schematic view of the interactions of MeAdoMet with the active-site residues is shown in Fig. 4.

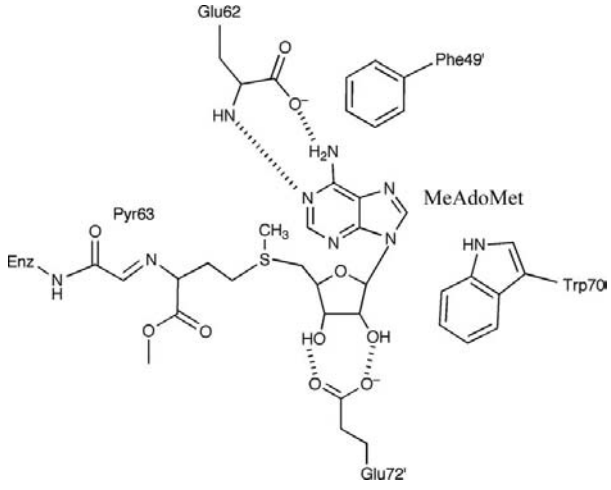

Figure 4
Schematic view of the interactions of MeAdoMet in the active site of TmAdoMetDC.

3.3. Complex with MMTA

The crystal structure of TmAdoMetDC complexed with MMTA was solved by molecular replacement. MMTA lacks the terminal nitrogen group necessary to form a Schiff base with the enzyme and is a competitive inhibitor. The difference $F_o - F_c$ maps show that MMTA binds to each of the twofold-related protomers. The enzyme undergoes side-chain conformational changes of residues Phe49′, His47′ and Tyr52′ upon MMTA binding as observed for MeAdoMet. The adenine base of MMTA also binds in the *syn* conformation with stacking against Phe49′. The 2′ and 3′ O atoms of the ribose make hydrogen bonds to the carboxylate group of Glu72′. The N1 atom of the adenine base makes a hydrogen bond to the amide group of Glu62. The carboxylate end of Glu62 is disordered in one protomer and shows two clear conformations in the other. The density for the carboxylate of Glu62 is too weak (Fig. 1*b*) to assign a second hydrogen bond to the N6 atom of the adenine base as seen in the MeAdoMet complex (Fig. 1*a*). The sulfonium ion is 4.3 Å from the CZ2 atom of the tryptophan ring, which is also the closest contact of the sulfonium with Trp70′. The cation–π interactions are similar to those of the MeAdoMet complex. The sulfonium ion is 4.5 Å away from the center of the six-membered ring of tryptophan. The methyl group on the sulfonium carries a partial positive charge and is 4.1 Å from the center of the Trp70′ ring and 3.6 Å from the CZ2 atom of the ring, which is also the closest contact of the methyl group with Trp70′. The sulfonium ion is 4.5 Å from the center of the Phe49′ ring and 4.0 Å from the CD2 and CE2 atoms of the ring, which is also the closest contact of the sulfonium ion with Phe49′. A stereoview of MMTA bound to TmAdoMetDC is shown in Fig. 3(*b*).

3.4. TmAdoMetDC kinetics

For TmAdoMetDC at 338 K, V_{max} was 4.3 pmol min^{-1} per nanogram of protein and K_m for AdoMet was 80 μM (Fig. 5).

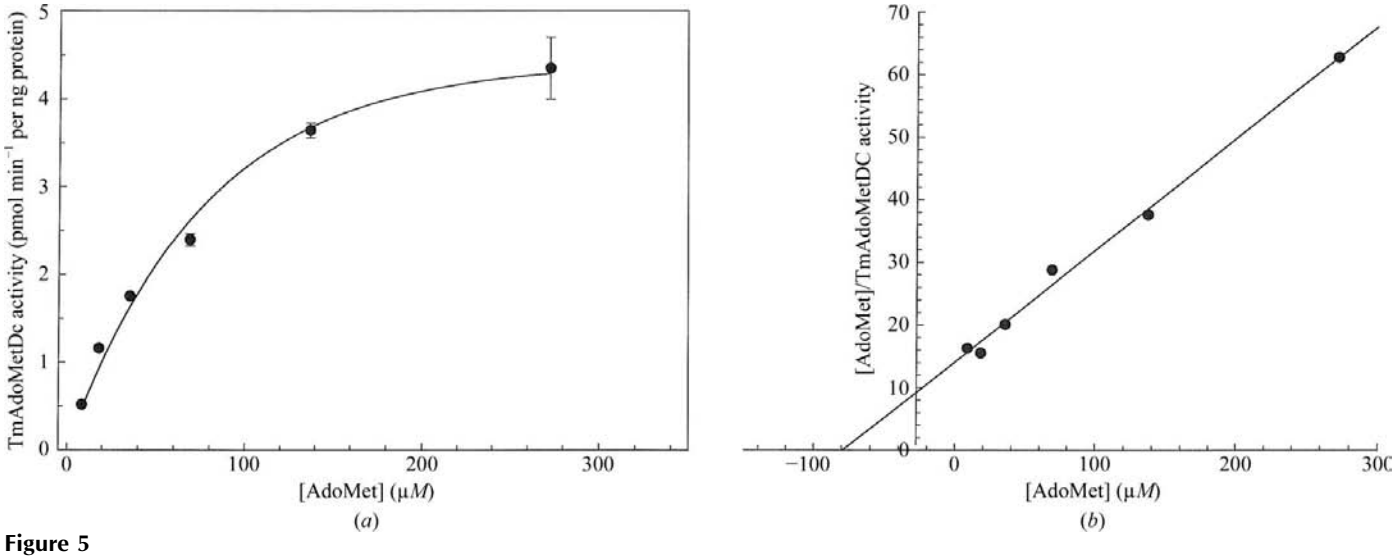

Figure 5
Kinetic measurements for TmAdoMetDC. (*a*) Determination of V_{max}. (*b*) Determination of K_m.

These values correspond to a k_{cat} of 1.0 s^{-1} and a k_{cat}/K_m of 1.25×10^4 s^{-1} M^{-1}.

4. Discussion

4.1. Processing of TmAdoMetDC

AdoMetDC is ubiquitously expressed as a proenzyme and undergoes internal serinolysis to mature to the active enzyme. Self-processing occurs between a glutamate and a serine residue, resulting in the formation of a pyruvoyl group derived from the serine residue. Processing occurs spontaneously in the human and potato enzymes, as seen in the crystal structures and supported by activity studies (Ekstrom *et al.*, 1999, 2001; Bennett *et al.*, 2002). Putrescine activates the processing and decarboxylation rates of hAdoMetDC (Ekstrom *et al.*, 2001; Bale *et al.*, 2008). Mechanical strain in the β-turn preceding the cleavage site has been implicated in autoprocessing in histidine decarboxylase and aspartate decarboxylase (Gallagher *et al.*, 1993; Schmitzberger *et al.*, 2003). The serine residue (Ser63) in TmAdoMetDC occurs in the fourth position of a β-turn. Processing was induced by heating the enzyme for 1 h at 353 K. The heat treatment for processing might be physiologically relevant as *T. maritima* are thermophilic bacteria with optimum growth at 353 K. This is the first study that proves unequivocally that the TmAdoMetDC proenzyme autoprocesses without additional factors. In all of the previous studies the protein processing occurred in the presence of other proteins and the limited amounts of wild-type proenzyme available were insufficient to demonstrate *in vitro* processing (Toms *et al.*, 2004). Comparison of the processed enzyme and the proenzyme revealed no significant changes in the secondary structure, suggesting that mechanical strain does not play a significant role in TmAdoMetDC.

The mechanism of processing of hAdoMetDC has been extensively studied using site-directed mutagenesis and crystal structures as reported previously (Ekstrom *et al.*, 2001; Tolbert *et al.*, 2003; Toms *et al.*, 2004). The conservation of active-site residues in TmAdoMetDC suggests that the mechanism of processing is similar. The hydroxyl group of Ser63 attacks the carbonyl C atom of the adjacent Glu62, resulting in the formation of an oxyoxazolidine intermediate. Deprotonation of the hydroxyl group would facilitate this step; however, there is no basic residue nearby. It is possible that Ser63 activation occurs *via* a water molecule. The oxyoxazolidine intermediate collapses to generate an ester intermediate. The amide H atom of Ser63 is abstracted by His68′, resulting in cleavage of the protein backbone into the α and β chains. The dehydroalanine residue at the N-terminus of the α chain undergoes tautomerization and subsequent hydrolysis to generate the pyruvoyl group.

4.2. Role of the sulfonium center in AdoMet binding

Biochemical studies have shown that substrate analogues lacking a positive charge do not bind to hAdoMetDC (Pegg & Jacobs, 1983; Pankaskie & Abdel-Monem, 1980). Consistent with this observation, substrate analogues that lack a positive charge at the sulfonium position have never been found in crystal structures. This has been attributed to favorable cation–π interactions between the sulfonium center and the aromatic rings of Phe223 and Phe7 (Bale *et al.*, 2009).

The complexes of TmAdoMetDC with MeAdoMet and MMTA revealed similar interactions to those seen in the human enzyme. The sulfonium center of MeAdoMet and MMTA is sandwiched between Trp70′ and Phe49′. The geometry and the distance of the sulfonium center from the aromatic rings are favorable for a cation–π interaction. Cation–π interactions in biology have been implicated in protein stability, ligand recognition, catalysis and ion channels (Gallivan & Dougherty, 1999; Ma & Dougherty, 1997; Zacharias & Dougherty, 2002). The strength of the interaction depends on the distance and the geometry of the cation from the aromatic ring and also on the nature of the cation and the interacting aromatic group. There are no negatively charged residues near the sulfonium center in AdoMetDC and the critical necessity of the positive charge for binding suggests that the cation–π interaction plays a significant role in ligand recognition in AdoMetDC (Bale *et al.*, 2009).

4.3. Stabilization of the AdoMet *syn* conformation

The adenine base of the ligand binds in an unusual *syn* conformation in hAdoMetDC. The base is sandwiched between Phe223 and Phe7 for favorable π-stacking interactions. The N6 and N1 atoms of the adenine base make two hydrogen bonds to the carboxylate and amide groups of the terminus of Glu67, respectively. The *syn* conformation is further stabilized by electrostatic interactions between the N3 atom of the base and the sulfonium center (Bale *et al.*, 2009). The crystal structure of the F223A mutant of hAdoMetDC shows that the adenine base still binds in the *syn* conforma-

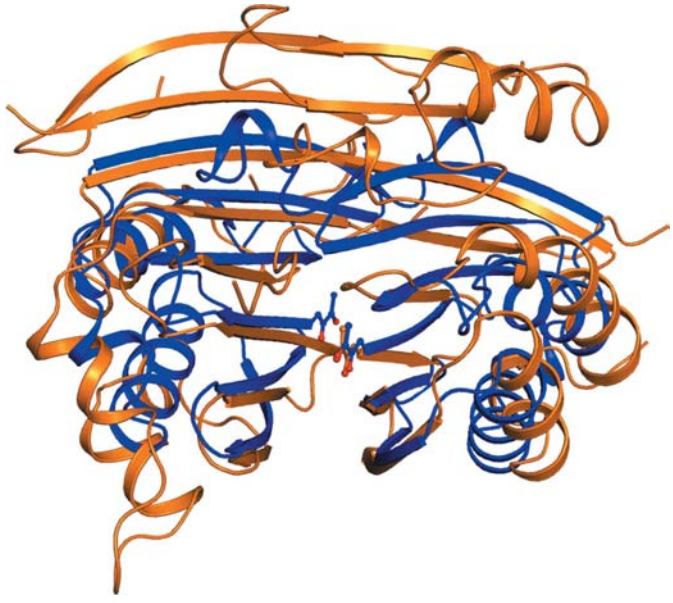

Figure 6
Superposition of the processed form of TmAdoMetDC (blue) and hAdoMetDC (orange). The pyruvoyl cofactor is shown in stick representation.

Table 3
Active-site residues in TmAdoMetDC and hAdoMetDC.

T. maritima†	Human	Role
Pyr63	Pyr68	Schiff base to the substrate
His68′	His243	Base for autoprocessing
Phe49′	Phe223	Stacking adenine base and sulfonium of substrate
Trp70′	Phe7	Stacking adenine base and sulfonium of substrate
Glu72′	Glu247	Hydrogen bonding to ribose moiety of substrate
Cys83	Cys82	Acid for decarboxylation
Glu62	Glu67	Hydrogen bonding to adenine base of substrate
Ser55′	Ser229	Positioning base for autoprocessing

† Residues labelled with a prime are from the twofold-related protomer.

Table 4
Comparison of residues in the second 'active' site.

Ser73 and Arg76 are positioned in a similar position to His68. Missing residues in equivalent positions are indicated by a dash.

T. maritima	Human	Role
Ser63	Thr238	Pyruvoyl group-forming residue
Glu62	Gly237	Residue in the β-turn
Ser61	Asp236	Residue in the β-turn
—	Ser235	Residue in the β-turn
Ile60	Lys234	Residue in the β-turn
Val59	Met233	Residue in the β-turn
His68	Ser73/Arg76	Base for processing
Ser55	Gln60	Base for processing
Cys83	—	Acid for decarboxylation

tion, suggesting that π-stacking to Phe7, hydrogen bonding to Glu67 and electrostatic effects are sufficient to stabilize the adenine base in the higher energy conformation (McCloskey *et al.*, 2009).

Both of the ligands MeAdoMet and MMTA bind to TmAdoMetDC in the high-energy *syn* conformation. The *syn* conformation is stabilized by π–π interactions with Phe49′. The adenine base is positioned edge-to-face 5.4 Å away from Trp70′ (the residue corresponding to Phe7 in hAdoMetDC) and does not have a favorable geometry or distance for stabilization by the aromatic ring. In the *syn* conformation, the N3 atom of the adenine base, which carries a partial negative charge, is 3.7 Å away from the positive charge of the sulfonium center in the MeAdoMet complex. In the MMTA complex, the distance between the corresponding atoms is 3.4 Å. This electrostatic interaction and hydrogen bonding to Glu62 further stabilize the *syn* conformation of the adenine base.

4.4. Implications for the evolution of AdoMetDC

The crystal structure of the processed form of TmAdoMetDC provides the first insight into substrate binding for a prokaryotic AdoMetDC. An evolutionary relationship for eukaryotic and prokaryotic AdoMetDCs has previously been proposed on the basis of overall structural similarity (Toms *et al.*, 2004). The conservation of active-site residues and of the structural basis for substrate specificity reported here adds further evidence for the evolution of AdoMetDC. TmAdoMetDC is a homodimer formed by two protomers related by twofold symmetry (Fig. 2*a*). Processing is observed in both protomers and the two active sites in the dimer are separated by ∼26 Å. Our studies clearly demonstrate that TmAdoMetDC contains two active sites. This is a significant difference from other solved structures and from the trypanosomal enzymes. Our study rules out the possibility that only one monomer processes and that the other monomer acts like a prozyme (Willert *et al.*, 2007). The human enzyme is a homodimer comprising of two ($\alpha\beta$) protomers. The N-terminal and C-terminal halves of hAdoMetDC are structurally homologous to each other and also to the protomer of TmAdoMetDC, suggesting that the human enzyme evolved by gene duplication and fusion. A superposition of the processed form of TmAdoMetDC and hAdoMetDC is shown in Fig. 6. Close overlap occurs (r.m.s.d. = 2.1 Å) even though TmAdoMetDC shows only 13% sequence identity to the N-terminal half of hAdoMetDC and 15% identity to the C-terminal half. The human enzyme contains two extra β-strands extending the central β-sheet in both the N-terminal half and the C-terminal half when compared with TmAdoMetDC. These β-strands form the dimer interface in the human enzyme.

The complexes of TmAdoMetDC with MeAdoMet and MMTA further elucidate the role of the active-site residues in binding the substrate as well as in the autoprocessing and decarboxylation reactions. Comparison of the active sites (Fig. 7) reveals the absolute conservation of the residues involved in the autoprocessing and decarboxylation processes in both the enzymes (Table 3). The comparison suggests key catalytic roles for residues Ser55, Ser63, His68 and Cys83. The only active-site difference is Trp70, which corresponds to a phenylalanine residue in the human enzyme. The change from one aromatic residue to another conserves the role of the side chain in stacking with the adenine base of the substrate. In hAdoMetDC the active site in the C-terminal half of the chain is lost; the essential Glu-Ser motif is Thr-Phe, the residues essential for substrate binding and catalysis are different and there is a one-amino-acid insertion in the β-turn Lys234–

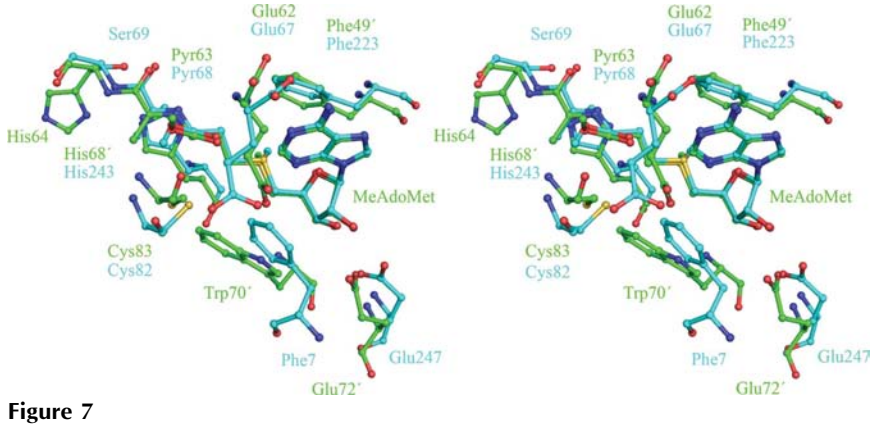

Figure 7
Stereoview of a comparison of the active sites of TmAdoMetDC (C atoms colored green) and hAdoMetDC (C atoms colored cyan) with MeAdoMet bound. Hydrogen bonds are omitted for clarity.

Thr238. A comparison of the residues in both the enzymes and their roles is shown in Table 4.

Evolutionary divergence has resulted in hAdoMetDC containing two protomers with a total molecular weight of 78 kDa, while TmAdoMetDC contains two protomers and has a total molecular weight of 28 kDa. Both enzymes have two active sites; however, gene duplication and fusion followed by the loss of one active site per protomer accounts for the larger size of the human enzyme. Interestingly, the efficiency of putrescine-stimulated hAdoMetDC (Xiong *et al.*, 1999) is only twofold higher than that of TmAdoMetDC (k_{cat}/K_m of $2.57 \times 10^4\ s^{-1}\ M^{-1}$ compared with $1.25 \times 10^4\ s^{-1}\ M^{-1}$ at 338 K for TmAdoMetDC), although the efficiency of the latter would be expected to increase at 353 K, which is the growth temperature of *T. maritima*. The turnover number is higher for hAdoMetDC (k_{cat} of $3.6\ s^{-1}$ compared with $1.0\ s^{-1}$ for TmAdoMetDC), while K_m is lower for TmAdoMetDC (80 μM compared with 140 μM for hAdoMetDC). In the absence of putrescine K_m is about eightfold higher for the human enzyme, resulting in a significant decrease in efficiency. TmAdoMetDC is not stimulated by putrescine but contains a buried Arg112 which closely overlaps with putescine in the superposition of TmAdoMetDC and hAdoMetDC. This arginine residue is absolutely conserved in all AdoMetDCs from archaebacteria and Gram-positive bacteria, which are designated class IB AdoMetDCs (Toms *et al.*, 2004).

4.5. Implications for inhibitor design

Inhibition of the polyamine-biosynthetic pathway to lower polyamine levels is a promising therapeutic strategy for cancer and parasitic diseases. Several AdoMetDC inhibitors have been the subject of clinical trials (Millward *et al.*, 2005; Williams-Ashman & Schenone, 1972). The structure of hAdoMetDC has been used for the development of substrate-analogue inhibitors with IC_{50} values in the micromolar to nanomolar range (McCloskey *et al.*, 2009). The key interactions of the inhibitors with the active site of the enzyme include (i) hydrogen bonding to Glu247 and Glu67, (ii) stacking interactions with Phe7 and Phe223, (iii) cation–π interactions with Phe223 and Phe7 and (iv) interactions with the pyruvoyl group. The complexes of TmAdoMetDC reveal that the key interactions mentioned are also conserved in prokaryotes. A comparison of the active sites of TmAdoMetDC and hAdoMetDC is shown in Fig. 7.

Inhibitors of polyamine biosynthesis also have potential applications in the treatment of trypanosomiasis and other parasitic infections. The crystal structure of AdoMetDC from *T. brucei* (TbAdoMetDC), which could serve as a basis for structure-based drug design, has not yet been determined. It has recently been shown that TbAdoMetDC exists as a heterodimeric complex formed by the active enzyme and a catalytically inactive homologue termed the prozyme (Willert *et al.*, 2007). Sequence alignment of hAdoMetDC, TmAdoMetDC and TbAdoMetDC shows that residues Glu266, Tyr242, Phe28 and Glu85 in TbAdoMetDC are likely to be involved in substrate binding. Residues Glu266 and Glu85 are equivalent to Glu247 and Glu67, respectively, in hAdoMetDC, and to Glu72 and Glu62, respectively, in TmAdoMetDC. Residues Tyr242 and Phe28 are equivalent to Phe223 and Phe7, respectively, in hAdoMetDC and to Phe49 and Trp70, respectively, in TmAdoMetDC. The conservation of the catalytic and substrate-binding residues suggests that all three enzymes have similar active sites. The similarity also suggests that the active sites of TmAdoMetDC and hAdoMetDC might serve as templates for structure-based drug design prior to the availability of the structure of TbAdoMetDC.

This work was supported by a National Cancer Institute Grant (CA-094000 to SEE and CA-018138 to AEP). We thank Ms Leslie Kinsland for assistance in the preparation of this manuscript. We thank the staff of NE-CAT beamline 24-ID-E at the Advanced Photon Source for providing beamtime and assistance in data collection. We thank Dr Angela Toms for insightful discussions into the processing of TmAdoMetDC. This work is based upon research conducted at the North-eastern Collaborative Access Team beamlines of the Advanced Photon Source, supported by award RR-15301 from the National Center for Research Resources at the National Institutes of Health. Use of the Advanced Photon Source is supported by the US Department of Energy, Office of Basic Energy Sciences under Contract No. DE-AC02-06CH11357.

References

Bale, S., Brooks, W., Hanes, J. W., Mahesan, A. M., Guida, W. C. & Ealick, S. E. (2009). *Biochemistry*, **48**, 6423–6430.
Bale, S., Lopez, M. M., Makhatadze, G. I., Fang, Q., Pegg, A. E. & Ealick, S. E. (2008). *Biochemistry*, **47**, 13404–13417.
Bennett, E. M., Ekstrom, J. E., Pegg, A. E. & Ealick, S. E. (2002). *Biochemistry*, **41**, 14509–14517.
Brünger, A. T., Adams, P. D., Clore, G. M., DeLano, W. L., Gros, P., Grosse-Kunstleve, R. W., Jiang, J.-S., Kuszewski, J., Nilges, M., Pannu, N. S., Read, R. J., Rice, L. M., Simonson, T. & Warren, G. L. (1998). *Acta Cryst.* D**54**, 905–921.
Casero, R. A. Jr, Frydman, B., Stewart, T. M. & Woster, P. M. (2005). *Proc. West. Pharmacol. Soc.* **48**, 24–30.
Casero, R. A. Jr & Marton, L. J. (2007). *Nature Rev. Drug Discov.* **6**, 373–390.
DeLano, W. L. (2002). *The PyMOL Molecular Graphics System.* DeLano Scientific, San Carlos, California, USA.
Ekstrom, J. E., Matthews, I. I., Stanley, B. A., Pegg, A. E. & Ealick, S. E. (1999). *Structure*, **7**, 583–595.
Ekstrom, J. L., Tolbert, W. D., Xiong, H., Pegg, A. E. & Ealick, S. E. (2001). *Biochemistry*, **40**, 9495–9504.
Emsley, P. & Cowtan, K. (2004). *Acta Cryst.* D**60**, 2126–2132.
Frey, P. A., Hegeman, A. D. & Ruzicka, F. J. (2008). *Crit. Rev. Biochem. Mol. Biol.* **43**, 63–88.
Gallagher, T., Rozwarski, D. A., Ernst, S. R. & Hackert, M. L. (1993). *J. Mol. Biol.* **230**, 516–528.
Gallivan, J. P. & Dougherty, D. A. (1999). *Proc. Natl Acad. Sci. USA*, **96**, 9459–9464.
Gerner, E. W. & Meyskens, F. L. Jr (2004). *Nature Rev. Cancer*, **4**, 781–792.
Hackert, M. L. & Pegg, A. E. (1997). *Comprehensive Biological Catalysis*, edited by M. L. Sinnott, pp. 201–216. London: Academic Press.
Kleywegt, G. J. & Jones, T. A. (1998). *Acta Cryst.* D**54**, 1119–1131.

Ma, J. C. & Dougherty, D. A. (1997). *Chem. Rev.* **97**, 1303–1324.
McCloskey, D. E., Bale, S., Secrist, J. A. III, Tiwari, A., Moss, T. H. III, Valiyaveettil, J., Brooks, W. H., Guida, W. C., Pegg, A. E. & Ealick, S. E. (2009). *J. Med. Chem.* **52**, 1388–1409.
Millward, M. J., Joshua, A., Kefford, R., Aamdal, S., Thomson, D., Hersey, P., Toner, G. & Lynch, K. (2005). *Invest. New Drugs*, **23**, 253–256.
Otwinowski, Z. & Minor, W. (1997). *Methods Enzymol.* **276**, 307–326.
Pankaskie, M. & Abdel-Monem, M. M. (1980). *J. Med. Chem.* **23**, 121–127.
Pegg, A. E. (1988). *Cancer Res.* **48**, 759–774.
Pegg, A. E. & Jacobs, G. (1983). *Biochem. J.* **213**, 495–502.
Pegg, A. E., Xiong, H., Feith, D. & Shantz, L. M. (1998). *Biochem. Soc. Trans.* **26**, 580–586.
Schmitzberger, F., Kilkenny, M. L., Lobley, C. M., Webb, M. E., Vinkovic, M., Matak-Vinkovic, D., Witty, M., Chirgadze, D. Y., Smith, A. G., Abell, C. & Blundell, T. L. (2003). *EMBO J.* **22**, 6193–6204.
Shantz, L. M. & Pegg, A. E. (1998). *Methods Mol. Biol.* **79**, 45–50.
Tabor, C. W. & Tabor, H. (1984*a*). *Adv. Enzymol. Relat. Areas Mol. Biol.* **56**, 251–282.
Tabor, C. W. & Tabor, H. (1984*b*). *Annu. Rev. Biochem.* **53**, 749–790.
Tolbert, D. W., Ekstrom, J. L., Mathews, I. I., Secrist, J. A. III, Kapoor, P., Pegg, A. E. & Ealick, S. E. (2001). *Biochemistry*, **40**, 9484–9494.
Tolbert, W. D., Zhang, Y., Cottet, S. E., Bennett, E. M., Ekstrom, J. L., Pegg, A. E. & Ealick, S. E. (2003). *Biochemistry*, **42**, 2386–2395.
Toms, A. V., Kinsland, C., McCloskey, D. E., Pegg, A. E. & Ealick, S. E. (2004). *J. Biol. Chem.* **279**, 33837–33846.
Willert, E. K., Fitzpatrick, R. & Phillips, M. A. (2007). *Proc. Natl Acad. Sci. USA*, **104**, 8275–8280.
Williams-Ashman, H. G. & Schenone, A. (1972). *Biochem. Biophys. Res. Commun.* **46**, 288–295.
Xiong, H., Stanley, B. A. & Pegg, A. E. (1999). *Biochemistry*, **38**, 2462–2470.
Zacharias, N. & Dougherty, D. A. (2002). *Trends Pharmacol. Sci.* **23**, 281–287.